Heat and Mass Transfer 37 (2001) 243–250 © Springer-Verlag 2001

Simultaneous radiative and convective heat transfer in a variable porosity medium

P. Nagaraju, A. J. Chamkha, H. S. Takhar, B. C. Chandrasekhara

Abstract The flow of an incompressible grey fluid through a horizontal channel filled with a saturated medium of variable viscosity has been considered in this paper. Such flows in porous media have several applications in industrial processes. For the radiative effects a two flux model has been used in order to simplify the governing integro-differential equations for which closed-form solutions are not obtainable. The problem has been solved by employing a highly successful tri-diagonal, implicit, iterative, finite difference method. The effects of the pertinent parameters on the velocity and temperature distributions have been shown in several figures.

List of symbols

b, B	non dimensional numbers
b_1, b_2	empirical constants
c	empirical constant
C_p	specific heat of the fluid, J/kg K
d	empirical constant
d_p	particle diameter, m
D_e	hydraulic diameter, m
h	heat transfer coefficient, W/mK
H	height of the channel, m
K	absorption coefficient, m^{-1}
$k(y)$	variable permeability, m^2
L	length of the channel, m
N	ratio of conduction to radiation $(\lambda_f \beta/4\sigma T_0^3)$
Nu	Nusselt number
p	pressure
Pe	Peclet number, (RePr)
P_m	porous parameter, $(\sqrt{150}\, H/\varepsilon_0 d_p)$
Pr	Prandtl number, (ν/α)
q	total heat flux, W/m^2
q_r	radiative heat flux, W/m^2
q_r^+, q_r^-	radiative fluxes in the forward and backward directions, W/m^2
Re	Reynolds number, $(u_0 H/\nu)$
s	scattering coefficient, m^{-1}
T_0	temperature at the entrance of the channel, K
T_1, T_2	temperature at the lower and upper plates, K
u	velocity of the fluid, m/s
u_0	Darcy velocity, m/s
x, y	co-ordinates, m

Greek letters

α	thermal diffusivity $(\lambda_f/\rho C_p)$ m^2/s
β	extinction coefficient $(K+s)$ m^{-1}
β_0	aspect ratio, (H/s)
γ	non-dimensional number
$\varepsilon_1, \varepsilon_2$	emissivity of the plates
ε_0	mean porosity
η	dimensionless variable
$\theta, \theta_1, \theta_2$	dimensionless temperatures
λ_e	effective thermal conductivity, W/mK
λ_s, λ_f	thermal conductivity of the solid and the fluid, W/mK
μ	dynamic viscosity, kg/ms
ν	kinematic viscosity of the fluid, m^2/s
ρ	density of the fluid, kg/m^3
σ	Stefan's constant, W/m^2 K^4
τ_0	optical thickness, βH
ω_0	albedo-scattering parameter, s/β
ϕ	dimensionless velocity
Φ	dimensionless radiative flux
Φ^+, Φ^-	dimensionless forward and backward radiative fluxes
ξ	dimensionless co-ordinate in the horizontal direction

Received on 6 December 1999

P. Nagaraju
Department of Physics,
Vijaya College, Bangalore-560 004, India

A. J. Chamkha
Department of Mechanical Engineering, Kuwait University,
Safat-13060, Kuwait

H. S. Takhar (✉)
Department of Engineering
Manchester Metropolitan University
Manchester, M1 5GD, UK

B. C. Chandrasekhara
Department of Physics,
Bangalore University, Banglore-560 056, India

1 Introduction

The study of two dimensional flow of radiating fluid in a variable porosity medium has become increasingly important because of its nature and practical importance, especially in high temperature systems. Some of the engineering applications of this type of problems are; (i) the entrance region flows in large tube reactors, (ii) external flows along buried pipes in packed beds, (iii) fluidised beds and (iv) heat exchangers. Further, as reported by Yoshida et al. [1], a porous medium placed in a duct

converts the gas enthalpy into thermal radiation. This has been applied in various industrial furnaces, and has attained remarkable energy savings and combustion enhancement. There are numerous industrial situations that require an analysis of the interaction between a fluid layer and a fluid saturated porous medium such as porous bearings, porous heat pipes etc. Modelling of such systems requires an understanding of the convective–radiative interaction between the fluid layer and the adjacent permeable systems. Heat transfer by combined conduction, convection and radiation in an absorbing, emitting and scattering porous medium has been sparsely studied. A detailed review work on the convective and radiative heat transfer in porous media by Tien and Vafai [2] reveals that this type of problem has not been given much attention by the research workers despite its applications in furnaces, such as glass processing and other translucent materials.

The coupling between the convective and radiative heat transfer leads to intergro-differential equations, which are mathematically involved (see Bergquam and Seban [3]; Chan and Tien [4]; Vortmeyer et al. [5]; Tong and Tien [6]; Boulet et al. [7]). Hence an approximate method is generally employed to solve these equations. But, the most commonly used approximate method is the two-flux model, which was originally introduced by Schuster [8]. This model was extended by Chandrasekhara [9], Viskanta [10] and others by approximating the radiation field in terms of a number of streams. The same model has been used in the recent works of Ozisik [11], Siegel and Howell [12], Brewster and Tien [13, 14], Wang and Tien [15], Yucel and Bayazitoglu [6], Lee and Howell [17], Brewster and Patel [18], Guilbert et al. [19], Wu et al. [20], Chandrasekhara and Nagaraju [21], Lu et al. [22], and Petrov [23].

The present study presents a two dimensional analysis of thermal radiation along with conduction and convection in a variable porosity medium which has a bearing on the above mentioned applications.

2 Mathematical formulation

The geometry of the physical system consists of a horizontal channel filled with saturated porous medium (Fig. 1). In such a medium, the flow of an incompressible grey fluid is considered, which is capable of emitting, absorbing, and isotropically scattering. Further, it is considered that in the porous medium at $x = 0$, the temperature of the fluid is uniform and is equal to T_0 and the temperature of the plates are maintained at constant but different temperatures, T_1 and T_2. Based on the above considerations, the momentum and energy equations are written as follows:

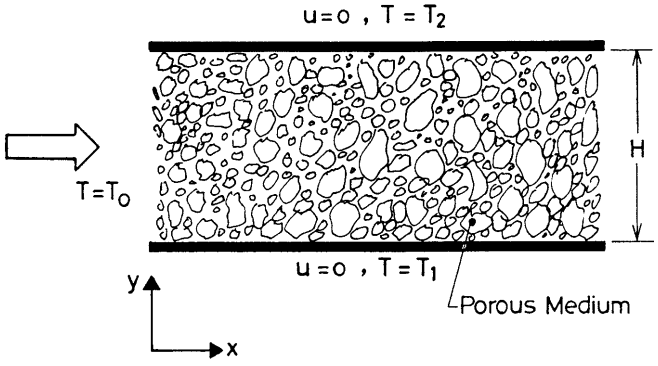

Fig. 1. Geometry and physical system

Momentum equation:

$$\frac{\mu}{\varepsilon(y)}\frac{\mathrm{d}^2u}{\mathrm{d}y^2} - \frac{\mu}{k(y)}u = \frac{\mathrm{d}p}{\mathrm{d}x} \tag{1}$$

where μ is the dynamic viscosity, $\varepsilon(y) = \varepsilon_0[1 + ce^{-(\mathrm{d}/\mathrm{d_p})y}]$ and $k(y) = \frac{\varepsilon^3(y)d_\mathrm{p}^2}{150[1-\varepsilon(y)]^2}$ are the expressions for variable porosity and permeability (Kozeny–Blake expression) respectively. Here ε_0 is the mean porosity and its value is chosen as 0.4, c and d are empirical constants which depend on the packing of spheres and d_p is the particle diameter. Equation (1) is the modified Darcy equation, also known as the Brinkman equation. In this equation, the dependent variables are all volumetric-averaged quantities.

Energy equation:

$$\rho C_p u\frac{\partial T}{\partial X} = \lambda_\mathrm{e}\frac{\partial^2 T}{\partial y^2} - \frac{\partial q_r}{\partial y} \tag{2}$$

where λ_e is the effective thermal conductivity, and $\partial q_r/\partial y$ is the radiative flux. The energy equation accounts for the conduction, convection and radiation models of energy transfer. It is to be noted that convection and radiation are the important mechanisms of energy transfer in fluidized bed system (Goshayeshi et al. [24]).

Radiative transfer equation:

$$q_\mathrm{r} = q_\mathrm{r}^+ - q_\mathrm{r}^- \tag{3}$$

where q_r^+ and q_r^- are the forward and backward radiation fluxes. Radiation transfer through a porous medium can be described in terms of an integro-differential equation called the transport equation, which is mathematically complicated, hence, a flux model is used for the sake of simplicity. Also when the channel is densely packed and the average diameter of the particles is small compared to the width of the channel, these two fluxes q_r^+ and q_r^- are related to each other through the set of non-linear ordinary differential equations.

$$\frac{\partial q_\mathrm{r}^+}{\partial y} = -2\beta(1-\omega_0 b_1)q_\mathrm{r}^+ + 2\beta\omega_0 b_2 q_\mathrm{r}^+ + 2\beta(1-\omega_0)\sigma T^4 \tag{4}$$

$$\frac{\partial q_\mathrm{r}^-}{\partial y} = 2\beta(1-\omega_0 b_1)q_\mathrm{r}^- - 2\beta\omega_0 b_2 q_\mathrm{r}^+ - 2\beta(1-\omega_0)\sigma T^4 \tag{5}$$

where $\beta\ (= K + s)$ is the extinction coefficient, $\omega_0 = s/\beta$ is the albedo-scattering parameter, b_1 and b_2 are empirical constants and σ is Stefan's constant. The radiative flux

divergence depends upon the temperature at each point throughout the medium and at the boundaries. Hence, the temperature distribution is very important in addition to the flux at the boundaries.

Boundary conditions:
For the momentum equation

$$u = 0 \quad \text{at } y = 0, H \tag{6a}$$

For the energy equation

$$\begin{aligned} &T(\text{at } x = 0) = T_0 \\ &T(\text{at } y = 0) = T_1 \\ &T(\text{at } y = H) = T_2 \end{aligned} \tag{6b}$$

For the radiative transfer equation

$$\begin{aligned} &q_{r1}^{+}(\text{at } y = 0) = \varepsilon_1 \sigma T_1^4 + (1 - \varepsilon_1) q_{r1}^{-} \\ &q_{r2}^{-}(\text{at } y = H) = \varepsilon_2 \sigma T_2^4 + (1 - \varepsilon_2) q_{r2}^{-} \ . \end{aligned}$$

Non dimensional quantities
The following non-dimensional parameters are introduced to solve the Eqs. (1)–(5)

$$\eta = \frac{y}{H}; \phi = \frac{u}{u_0}; \theta = \frac{T}{T_0}; \theta_1 = \frac{T_1}{T_0}; \theta_2 = \frac{T_2}{T_0}; \eta = \frac{\beta y}{\tau_0} \tag{7}$$

$$\Phi = \frac{q_r}{\sigma T_0^4}; N = \frac{\lambda_f \beta}{4\sigma T_0^3}; \xi = \frac{x}{L} \ .$$

Here $u_0 = -\frac{k(\eta)}{\mu}\frac{\mathrm{d}p}{\mathrm{d}x}$ is the Darcy velocity, T_0 is the temperature at the entrance of the channel, $\tau_o = \beta H$ is the optical thickness. Using non-dimensional parameters, Eq. (1) becomes

$$\frac{\mathrm{d}^2\phi}{\mathrm{d}\eta^2} - \frac{\varepsilon(\eta)}{k(\eta)} H^2 \phi = -\frac{\varepsilon(\eta) H^2}{k(\eta)} \tag{8}$$

where $\varepsilon(\eta) = \varepsilon_0\left[1 + c\mathrm{e}^{-\left(Hd/d_\mathrm{p}\right)\eta}\right]$ and $k(\eta) = \frac{\varepsilon^3(\eta) d_\mathrm{p}^2}{150[1-\varepsilon(\eta)]^2}$.
Equation (8) can now be rewritten as

$$\frac{\mathrm{d}^2\phi}{\mathrm{d}\eta^2} - \frac{150H^2}{\varepsilon^2(\eta) d_\mathrm{p}^2}[1 - \varepsilon(\eta)]^2 \phi = -\frac{150H^2[1 - \varepsilon(\eta)]^2}{\varepsilon^2(\eta) d_\mathrm{p}^2}$$

or

$$\frac{\mathrm{d}^2\phi}{\mathrm{d}\eta^2} - \frac{150H^2}{\varepsilon_0^2(\eta) d_\mathrm{p}^2} \frac{\left[1 - \varepsilon_0\left\{1 + c\mathrm{e}^{-\left(Hd/d_\mathrm{p}\right)\eta}\right\}\right]^2}{\left[1 + c\mathrm{e}^{-\left(Hd/d_\mathrm{p}\right)\eta}\right]^2} \phi = -\frac{150H^2}{\varepsilon_0^2 d_\mathrm{p}^2} \frac{\left[1 - \varepsilon_0\left\{1 + c\mathrm{e}^{-\left(Hd/d_\mathrm{p}\right)\eta}\right\}\right]^2}{\left[1 + c\mathrm{e}^{-\left(Hd/d_\mathrm{p}\right)\eta}\right]^2}$$

or

$$\frac{\mathrm{d}^2\phi}{\mathrm{d}\eta^2} - \frac{P_\mathrm{m}^2[1 - \varepsilon_0\{1 + c\mathrm{e}^{-d\gamma\eta}\}]^2}{[1 + c\mathrm{e}^{-d\gamma\eta}]^2}\phi = -\frac{P_\mathrm{m}^2[1 - \varepsilon_0\{1 + c\mathrm{e}^{-d\gamma\eta}\}]^2}{[1 + c\mathrm{e}^{-d\gamma\eta}]^2} \tag{9}$$

where $P_\mathrm{m}^2 = \left(\frac{150H^2}{\epsilon_0^2 d_\mathrm{p}^2}\right)$ is the porous parameter and $\gamma = H/d_\mathrm{p}$.

The porosity of the medium should remain the same at both boundaries, hence the non-dimensional momentum Eq. (9) is expressed in two different forms as follows:

$$\frac{\mathrm{d}^2\phi}{\mathrm{d}\eta^2} - \frac{P_\mathrm{m}^2[1 - \varepsilon_0\{1 + c\mathrm{e}^{-d\gamma\eta}\}]^2}{[1 + c\mathrm{e}^{-d\gamma\eta}]^2}\phi = -\frac{P_\mathrm{m}^2[1 - \varepsilon_0\{1 + c\mathrm{e}^{-d\gamma\eta}\}]^2}{[1 + c\mathrm{e}^{-d\gamma\eta}]^2} \tag{10a}$$

in the interval $0 \le \eta \le 1/2$, and

$$\frac{\mathrm{d}^2\phi}{\mathrm{d}\eta^2} - \frac{P_\mathrm{m}^2[1 - \varepsilon_0\{1 + c\mathrm{e}^{-d\gamma(1-\eta)}\}]^2}{[1 + c\mathrm{e}^{-d\gamma(1-\eta)}]^2}\phi = -\frac{P_\mathrm{m}^2[1 - \varepsilon_0\{1 + c\mathrm{e}^{-d\gamma(1-\eta)}\}]^2}{[1 + c\mathrm{e}^{-d\gamma(1-\eta)}]^2} \tag{10b}$$

in the interval $1/2 \le \eta \le 1$.

It is to be noted that; in the interval $0 \le \eta \le 1/2$

$$\varepsilon(\eta) = \varepsilon_0[1 + c\mathrm{e}^{-d\gamma\eta}] \tag{11a}$$

and in the interval $1/2 \le \eta \le 1$

$$\varepsilon(\eta) = \varepsilon_0[1 + c\mathrm{e}^{-d\gamma(1-\eta)}] \ . \tag{11b}$$

Equations (11a) and (11b) yield $\varepsilon(\eta) = \varepsilon_0(1 + c)$ for $\eta = 0$ and $\eta = 1$ respectively. This makes the porosity maximum at the walls, as it should be. Both the expression [Eqs. (11a, 11b)] reduce the porosity to a minimum value at $\eta = 1/2$, i.e. is $\varepsilon(1/2) = \varepsilon_0[1 + c\mathrm{e}^{-\mathrm{d}\gamma/2}]$. This makes the porosity minimum along the axis of the channel.

Equation (2) in the non-dimensional form is written as

$$\rho C_p u_0 \phi(\eta) \frac{T_0}{L} H^2 \frac{\partial\theta}{\partial\xi} = \lambda_\mathrm{e} T_0 \frac{\partial^2\theta}{\partial\eta^2} - \frac{\sigma T_0^4}{H}\frac{\partial\Phi}{\partial\eta}$$

or

$$\frac{\partial^2\theta}{\partial\eta^2} = \frac{\sigma T_0^3 H}{\lambda_\mathrm{e}}\frac{\partial\Phi}{\partial\eta} + \frac{\rho C_p u_0 H^2}{\lambda_\mathrm{e} L}\phi(\eta)\frac{\partial\theta}{\partial\xi} \ . \tag{12}$$

Equations (3) and (4) can now be written in the non-dimensional form as follows:

$$\begin{aligned} \frac{\partial\Phi^+}{\partial\eta} &= -2\tau_0(1 - \omega_0 b_1)\Phi^+ + 2\tau_0\omega_0 b_2\Phi^- \\ &\quad + 2\tau_0(1 - \omega_0)\theta^4 \end{aligned} \tag{13}$$

$$\frac{\partial\Phi^-}{\partial\eta} = 2\tau_0(1 - \omega_0 b_1)\Phi^- - 2\tau_0\omega_0 b_2\Phi^+ - 2\tau_0(1 - \omega_0)\theta^4. \tag{14}$$

The definition of the radiative flux yields;

$$\begin{aligned} \frac{\partial\Phi}{\partial\eta} &= 2\tau_0[-(\Phi^+ + \Phi^-)(1 - \omega_0 b_1 - \omega_0 b_2) \\ &\quad + 2(1 - \omega_0)\theta^4] \end{aligned} \tag{15}$$

From Eqs. (12) and (15), one can get

$$\frac{\partial^2\theta}{\partial\eta^2} = \frac{\tau_0^2}{2NA}\left[-(\Phi^+ + \Phi^-)(1-\omega_0 b_1 - \omega_0 b_2) + 2(1-\omega_0)\theta^4\right] + \frac{\mathrm{Pe}\beta_0}{A}\phi(\eta)\frac{\partial\theta}{\partial\xi} \tag{16}$$

where $\mathrm{Pe} = \mathrm{RePr}$; $\mathrm{Re} = \frac{u_0 H}{\nu}$; $\mathrm{Pr} = \frac{\nu}{\alpha}$; $\alpha = \frac{\lambda f}{\rho C_p}$; $\beta_0 = \frac{H}{L}$; $\tau_o = \beta H$; and $N = \frac{\lambda_f \beta}{\sigma T_1^3}$.

The effective thermal conductivity λ_e is taken (after Zehner and Schlunder [25]) as $\lambda_e = \lambda_f A$, where

$$A = \left\{1 - \sqrt{1-\varepsilon(\eta)}\right\} + \frac{2\sqrt{1-\varepsilon(\eta)}}{\left(1-\frac{B}{b}\right)} \times \left\{\frac{\left(1-\frac{1}{b}\right)}{\left(1-\frac{B}{b}\right)^2}\ln\frac{b}{B} - \left(\frac{B+1}{2}\right) - \frac{(B-1)}{\left(1-\frac{B}{2}\right)}\right\}$$

and

$$b = \frac{\lambda_s}{\lambda_f} = \frac{\text{thermal conductivity of the solid}}{\text{thermal conductivity of the fluid}};$$

$$B = 1.25\left[\frac{1-\varepsilon(\eta)}{\varepsilon(\eta)}\right]^{10/9}.$$

The transformed boundary conditions are written as follows:

Momentum:

$$\phi = 0 \text{ at } \eta = 0 \text{ and } \eta = 1 \tag{16a}$$

Energy:

$$\theta \text{ (at } \xi = 0) = \theta_0 \tag{16b}$$

$$\theta \text{ (at } \eta = 0) = \theta_1 \tag{16c}$$

$$\theta \text{ (at } \eta = 1) = \theta_2 \tag{16d}$$

Radiative transfer:

$$\Phi_1^+ \text{ (at } \eta = 0) = \varepsilon_1\theta_1^4 + (1-\varepsilon_1)\Phi_1^- \tag{16e}$$

$$\Phi_2^- \text{ (at } \eta = 1) = \varepsilon_2\theta_2^4 + (1-\varepsilon_2)\Phi_2^+ \ . \tag{16f}$$

The total wall heat flux is determined in terms of the conventional definition of the Nusselt number, which is defined for the present problem, as

$$\mathrm{Nu} = \frac{hD_e}{\lambda_e} = \frac{qD_e}{\lambda_e(T_1 - T_0)} = \frac{2H\left(-\lambda_e\frac{\mathrm{d}T}{\mathrm{d}y} + q_r\right)_{y=0}}{\lambda_e(T_1 - T_0)} \tag{17}$$

It is to be noted that the equivalent diameter D_e is equal to $2H$. The expression for the Nusselt number in terms of dimensionless variables becomes

$$\mathrm{Nu} = \frac{2\tau_0\left(-\frac{1}{\tau_0}\frac{\mathrm{d}\theta}{\mathrm{d}\eta} + \frac{\Phi}{4NA}\right)_{\eta=0}}{(\theta_1 - \theta_0)} = \frac{2\left(-\frac{\mathrm{d}\theta}{\mathrm{d}\eta} + \frac{\tau_0}{4NA}\Phi\right)_{\eta=0}}{(\theta_1 - \theta_0)} \tag{18}$$

3 Solution method

Equations(10)–(15) are obviously non-linear and no closed form solution can be obtained subject to the boundary conditions given in Eqs. (16a–16f). Therefore, these must be solved numerically. The tri-diagonal, implicit, interative, finite difference method discussed by Blottner [26] and Patankar [27] has proven to be successful in the solution of boundary layer type problems. For this reason, it is adopted in the present work.

The problem is solved numerically for the functions ϕ, θ, Φ^+ and Φ^-. The equation for the hydrodynamic flow velocity ϕ, involves two different expressions for the variation of porosity in the region $0 \le \eta \le 1/2$ and $1/2 \le \eta \le 1$. But, the equations for the functions θ, Φ^+ and Φ^- do not involve such expressions, and hence these are integrated straightaway in the internal $0 \le \eta \le 1$. There are only two boundary conditions for ϕ and it has to be supplemented by the continuity condition at $\eta = 1/2$. Equation (10a) is to be integrated from the end $\eta = 0$ and should be carried on till the point $\eta = 1/2$ is reached. Equation (10b) is to be integrated from the point $\eta = 1$ and should be carried on till $\eta = 1/2$ is reached. The value of $\mathrm{d}\phi/\mathrm{d}\eta$ at $\eta = 1/2$ obtained by both the integrations should be the same. Further, it is seen from the governing equations that the hydrodynamic flow velocity (ϕ) is independent of the axial distance ξ, while the thermal flow is dependent on ξ through the term $\partial\theta/\partial\xi$ appearing in Eq. (16). Therefore, the problem is solved as an initial-value problem, with ξ playing the role of time. All second order differential equations in η are discretized using the three-point central difference quotients while all the first order differential equations in η are discretized using the trapezoidal rule. The computational domain was divided into 101 nodes in the ξ direction and 201 nodes in the η direction. Constant step sizes in the η and ξ directions, with $\Delta\eta = 0.005$ and $\Delta\xi = 0.01$, are used. The governing equations are then converted into sets of linear tri-diagonal algebraic equations, which are solved by using the Thomas Algorithm (see Blottner [26]) at each iteration. The convergence criterion employed herein required that the difference between the current and the previous iterations to be 10^{-5}. It should be mentioned that many numerical experimentation were performed by altering the step sizes in both the directions to ensure the accuracy of the results and to assess the grid independence. Equations (10)–(14) were first solved for ϕ, Φ^+ and Φ^-, then the solution of θ is obtained. Once all profiles are obtained at a certain ξ location, then the solution procedure is repeated at the next ξ locations down stream of the channel.

4 Results and discussion

The problem under consideration is governed by the porous parameter (P_m), optical thickness (τ_0), Peclet number (Pe), albedo-scattering parameter (ω_0), conduction to radiation parameter (N) and the ratio of the temperatures θ_2/θ_1. In this paper the values of non-dimensional numbers are chosen with air as the reference fluid. For example, the Peclet number Pe is taken from 10–10^4 and the porous parameter P_m from 153–306. One should note that

the numerical value of P_m is based on the width of the channel H and the particle diameter d_p. For a typical channel of width 10 cm and particle diameter 1 cm, the ratio $H/d_p(=\gamma)$ becomes 10. The mean porosity ε_0 far from the plates is taken as 0.4, and the constants c and d are so chosen such that the porosity at the plates becomes unity. For different values of γ(5 to 10) the values of P_m turn out to be 153 to 306. Thus, the problem is solved numerically for different combinations of parameters.

Figure 2 shows the velocity distribution for different values of P_m. As expected, the velocity profile is symmetric at both the boundaries and exhibits the wall-channelling effect due to high porosity near the plates. Further, it exhibits the flattering effect in between the two plates. One interesting feature to be observed in this figure is the decrease in the peak velocity with an increase in P_m. This is due to the fact that the resistance offered by the solid material increases with an increase in P_m and thus the flow is retarded. Figure 3 shows the effect of temperature θ_2 on the dimensionless temperature function θ, as θ_2 is increased from 0.1 to 1.0. When both the plates are at the same temperature $(\theta_1 = \theta_2 = 1)$ there exists an equilibrium condition. The effect of P_m on the temperature distribution is indicated in Fig. 4. As reported by Nagaraju [28], with an increase in the value of P_m from 35 to 50, the percentage increase in θ at $\eta - 0.5$ is about 18%, whereas, for an increase in the value of P_m from 50 to 80, it is about 12%. This shows that the percentage increase in temperature tends to a constant after a certain value is reached. In this investigation the values of P_m are taken large and hence the temperature distribution remains the same for all values of P_m. Figure 5 illustrates the effect of the albedo-scattering parameter ω_0 on the temperature distribution. The limit $\omega_0 = 0$ denotes a non- scattering medium, while $\omega_0 = 1$ a pure scattering medium. In the pure scattering medium, the energy equation is uncoupled from the radiation transfer process, and in turn, the radiation transfer is independent of the temperature field within the medium. Indeed, the influence of ω_0 is not dominant due to the large packing of the solid materials. However, its effect cannot be neglected, for instance the temperature level decreases as ω increases from 0 to 1.

The effect of the optical thickness τ_0 on the temperature distribution is illustrated in Fig. 6. As τ_0 increases the

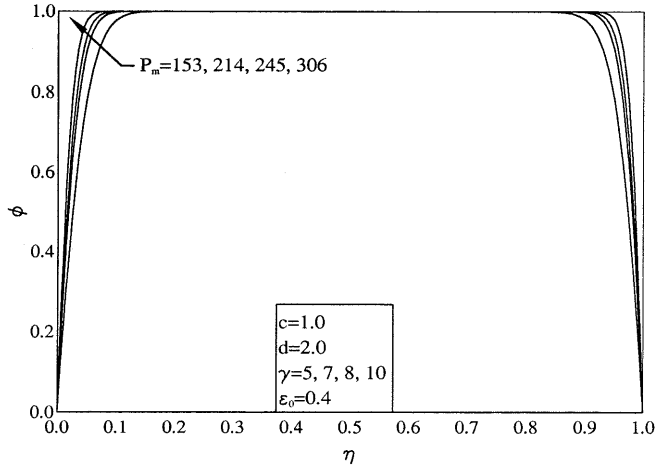

Fig. 2. Effect of P_m on velocity profile

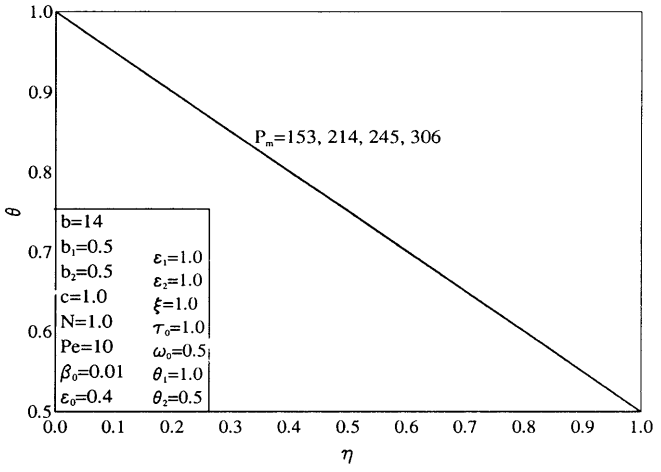

Fig. 4. Effect of P_m on temperature distribution

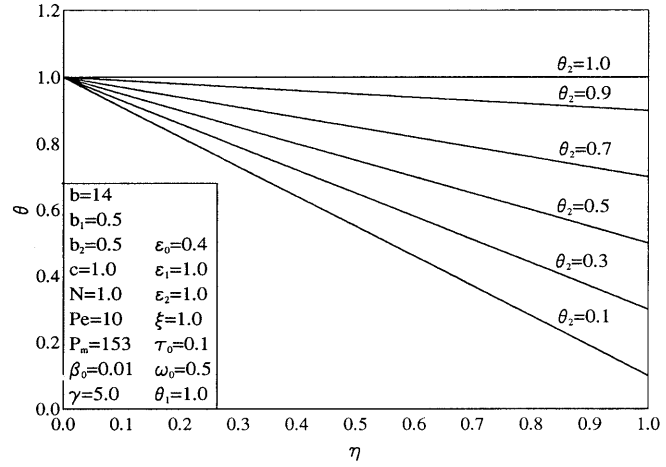

Fig. 3. Temperature distribution for different θ_2

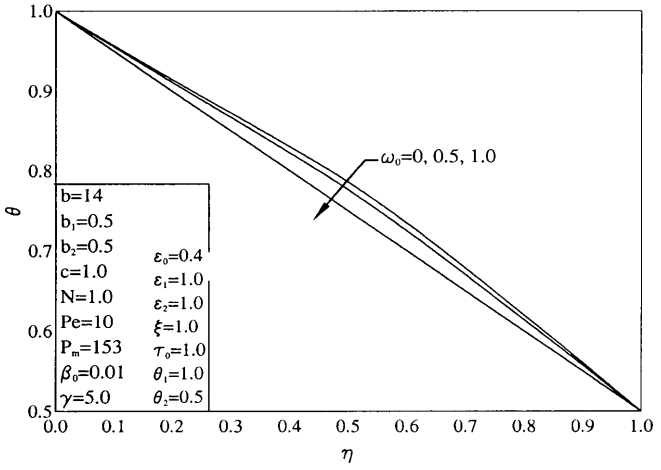

Fig. 5. Effect of ω_0 on temperature distribution

temperature increases in the middle of the channel. The effect of the parameter N, which is defined as the ratio of conduction to radiation heat transfer is shown in Fig. 7. It is seen from this figure that as N increases, the temperature level decreases. For lower values of N (0.1, 0.5) the temperature profile is non-linear indicating that radiation is dominant in the heat transfer process. However, as the value of N (=10) increases conduction takes over together with convection and the heat is transferred from the plates to the fluid and the profile becomes symmetric and almost linear.

Figure 8 shows that the radiation transfer increases with an increase in P_m. The effect of N on local radiation flux is presented in Fig. 9, which shows that as N increases the local radiation flux decreases. For example, when $N = 0.1$, the radiation is dominant over conduction, and hence the heat transfer due to radiation is more dominant, but when $N = 10$, the conduction is dominant over radiation and hence the conduction effect is more more pronounced. The local dimensionless radiation flux Φ is shown in Fig. 10 with τ_0 as a parameter. It must be noted that the radiation flux at the wall is always lower than in the vicinity of the wall. Physically, Φ is lower at the wall because the conduction and convection force the fluid temperature adjoining the wall to equal the wall temperature and thereby reduce the radiation flux at the wall. It is seen that Φ is quite flat between the two plates for small values of the optical thickness (0.1), but, it becomes less uniform as τ_0 increases (> 10). Figure 11 reveals the effect of the

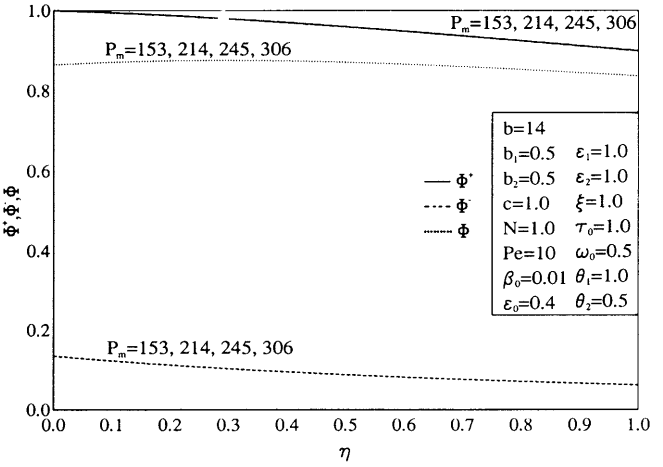

Fig. 8. Effect of P_m on Φ^+, Φ^- and Φ

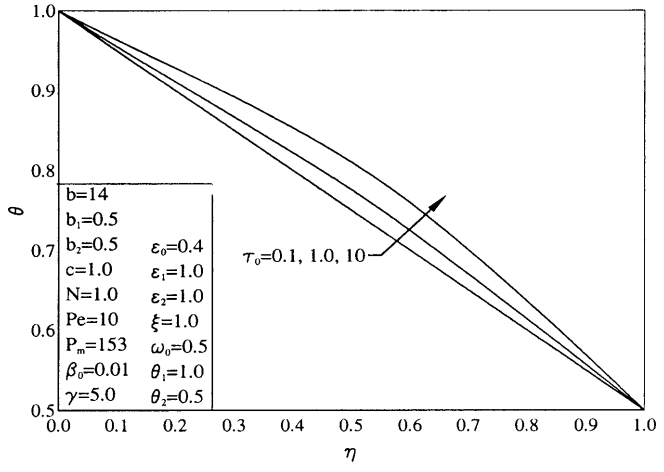

Fig. 6. Effect of τ_0 on temperature distribution

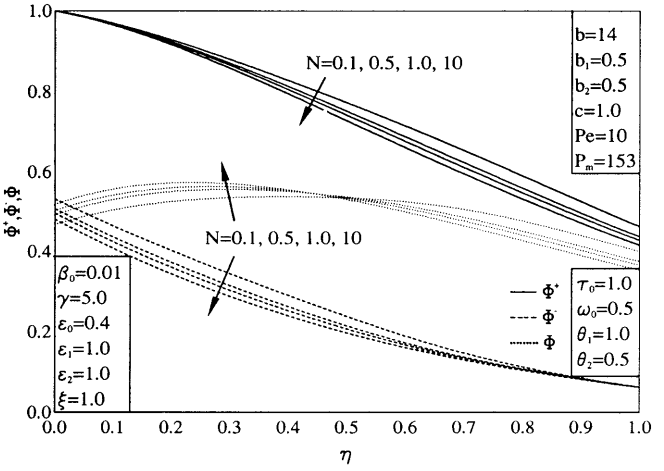

Fig. 9. Effect of N on Φ^+, Φ^- and Φ

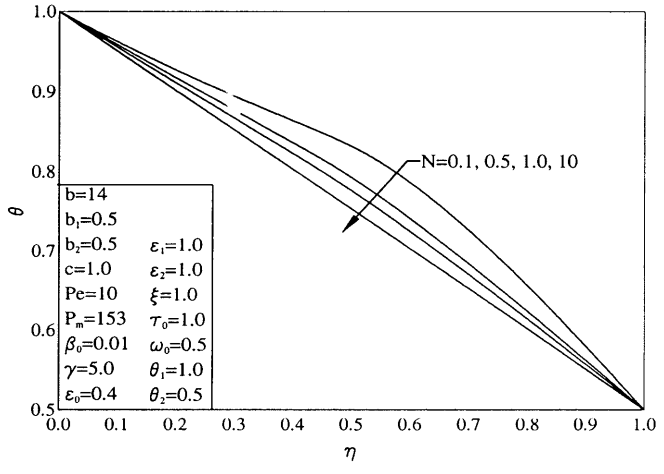

Fig. 7. Effect of N on temperature distribution

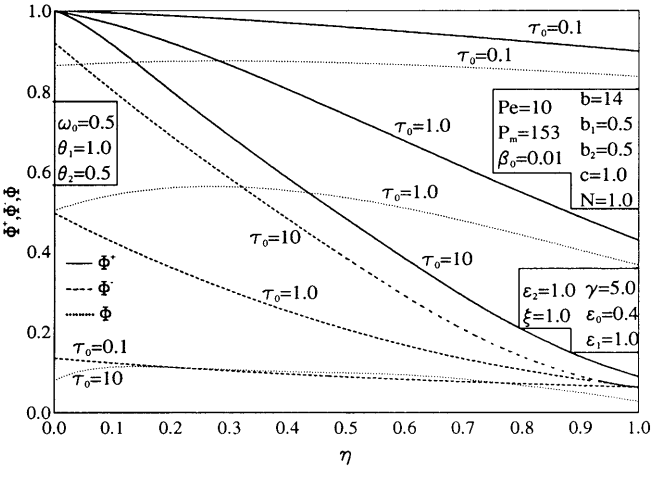

Fig. 10. Effect of τ_0 on Φ^+, Φ^- and Φ

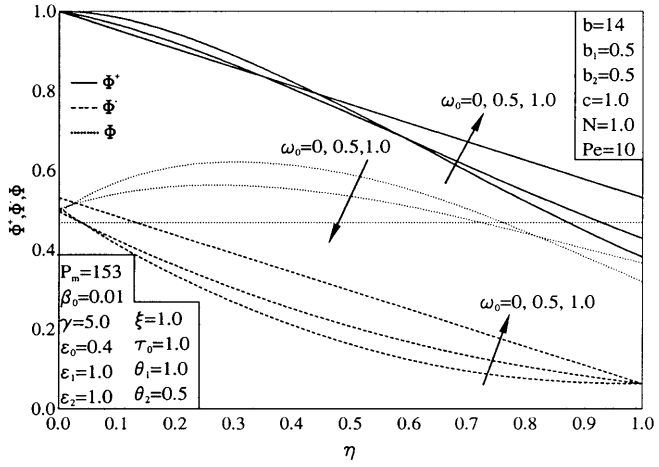

Fig. 11. Effect of ω_0 on Φ^+, Φ^- and Φ

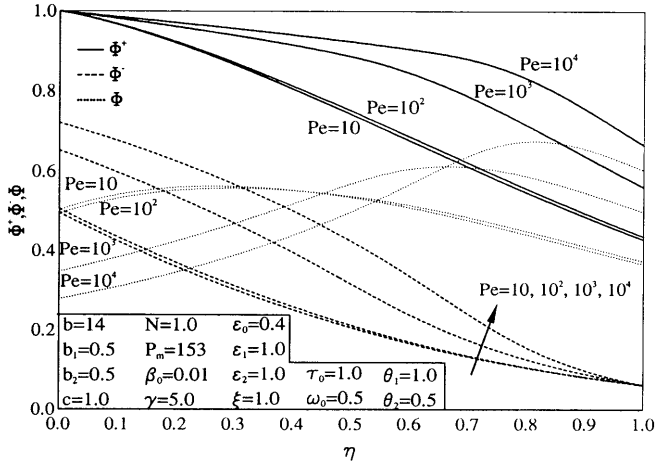

Fig. 12. Effect of Pe on Φ^+, Φ^- and Φ

albedo-scattering parameter ω_0 on Φ^+, Φ^- and Φ. It is to be noted that an increase in the albedo-scattering parameter decreases the radiation flux at the wall. The effect of the Peclet number Pe is shown in Fig. 12. It is evident that for a small Peclet number, the temperature of the fluid sharply drops, and hence the radiative flux decreases sharply.

Figure 13 illustrates the effect of the various parameters on the Nusselt number Nu. As expected, the wall heat transfer, represented by Nu, is seen to decrease with an increasing value of ξ. Also, Nu is predicted to increase, with increases of either ω_0, N or Pe and a decrease in either of b, τ_0, or θ_2. The parametric values for which the reference curve is obtained are given on this figure.

5 Conclusions

1. The peak velocity between the plates decreases with increasing values of the porous parameter P_m, but the radiative transfer increases with an increase in P_m.
2. The influence of albedo-scattering parameter ω_0 is not dominant due to the large packing of the solid material. However its effect is not negligible, for instance the temperature level decreases as ω_0 increases from 0 to 1.

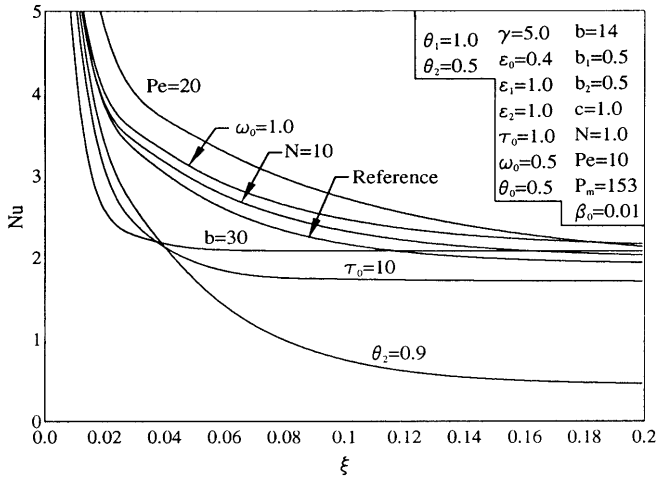

Fig. 13. Development of Nusselt number

3. The optical thickness parameter τ_0 increases as the temperature increases in the middle of the channel.
4. As the ratio of conduction to radiation parameter N increases as the temperature level decreases. For lower values of N the radiation process is dominant, while for large N conduction together with convection takes over. Also as N increases the local radiation flux decreases.
5. For small values of the Peclet number the temperature of the fluid drops sharply, and so too the radiative fluxes.
6. The Nusselt number Nu decreases with increasing values of the axial distance ξ. It increases with an increase in either of ω_0, N or Pe and a decrease in either of b, τ_0 or θ.

References

1. **Yoshida H; Yun JH; Echigo R** (1990) Transient characteristics of combined conduction, convection and radiation heat transfer in porous media. Int J Heat Mass Transfer 33: 847–857
2. **Tien CL; Vafai K** (1990) Convective and radiative heat transfer in porous media. Adv Appl Mech 27: 225–281
3. **Bergquam JB; Seban RA** (1971) Heat transfer by conduction and radiation in absorbing and scattering materials. ASME J Heat Transfer 93: 236–239
4. **Chan CK; Tien CL** (1974) Radiative transfer in packed sphere. ASME J Heat Transfer 96: 52–58
5. **Vortmeyer D; Rudraiah N; Sasi Kumar TP** (1989) Effect of radiative transfer on the onset of convection in a porous medium. Int J Heat Mass Transfer 32: 873–879
6. **Tong TW; Tien CL** (1983) Radiative heat transfer in fibrous insulations, Part I, analytical study. ASME J Heat Transfer 105: 70–75
7. **Boulet P; Jeandel G; Morlot G** (1993) Model of radiative transfer in fibrous media matrix method. Int J Heat Mass Transfer 36: 4287–4297
8. **Schuster A** (1905) Radiation through a foggy atmosphere. Astrophysical J 21: 1–22
9. **Chandrasekhara S** (1960) Radiative Transfer, Dover, New York
10. **Viskanta R** (1965) Heat transfer by conduction and radiation in absorbing and scattering materials. ASME J Heat Transfer 87: 143–150

11. **Ozisik MN** (1973) Radiative Transfer and Interactions with Conduction and Convection, Wiley, New York
12. **Siegel R; Howell RJ** (1981) Thermal Radiation Transfer (2nd edn.), Hemisphere, New York
13. **Brewster MQ; Tien CL** (1982) Examination of the two flux model for radiative transfer in particular systems. Int J Heat Mass Transfer 25: 1905–1907
14. **Brewster MQ; Tien CL** (1982) Radiative transfer in packed fluidized beds; Dependent versus independent scattering. ASME J Heat Transfer 104: 573–579
15. **Wang KY; Tein CL** (1983) Radiative transfer through optical fibres and powders. J Quan Spectro Radiative Transfer 30: 213–223
16. **Yücel A; Bayazitoglu Y** (1984) Radiative heat transfer in absorbing, emitting and anisotropically scattering boundary-layer flows. AIAA J 22: 1162–1166
17. **Lee KB; Howell JR** (1986) Effect of radiation on the laminar convective heat transfer through a layer of highly porous medium. In: Tong T, Modest M (eds) Radiation in Energy Systems, ASME HTD Vol. 55, pp. 51–59
18. **Brewster MQ; Patel R** (1987) Selective radiative preheating of aluminium in composite solid propellant combustion. ASME J Heat Transfer 109: 179–184
19. **Guilbert G; Jeandel G; Morlot G; Langlais C; Klarsfild S** (1987) Optical characteristics of semi-transparent porous media. High Temp High Press 19: 251–259
20. **Wu CY; Wu SC; Chen CK** (1989) Radiative heat transfer in anisotropically scattering boundary-layer flows with diffusely reflecting boundaries. In: Lewis RW, Morgan K (eds) Numerical Methods in Thermal Problems. Proceedings of the 6th International Conference, pp. 773–779
21. **Chandrasekhara BC; Nagaraju P** (1993) Composite heat transfer in a variable porosity medium bounded by an infinite flat plate. Heat and Mass Transfer 28: 449–456
22. **Lu JD; Flamant G; Variot G** (1994) Theoretical study of combined conductive, convective and radiative flow between plates and packed beds. Int J Heat Mass Transfer 37: 727–737
23. **Petrov VA** (1997) Combined radiation and conduction heat transfer in high temperature fibre thermal insulations. Int J Heat Mass Transfer 40: 2241–2247
24. **Goshayeshi A; Wetty JR; Adams RL; Alvizadeh N** (1968) Local heat transfer coefficients for horizontal tube arrays in high temperature large particle fluidized beds. An experimental study. ASME J Heat Transfer 108: 907–912
25. **Zehner P; Schlunder EV** (1970) Waermeleitfahigkeit von Schllettungenei massigen Temperatureu. Chie, Ingr-Tech 22: 933–941
26. **Blottner F** (1970) Finite difference methods of solutions of the boundary layer equations. AIAA J 8: 193–205
27. **Patankar SV** (1980) Numerical Heat Transfer in Fluid Flow, McGraw-Hill, New York
28. **Nagaraju P** (1993) Composite heat transfer problems in saturated porous media. PhD Thesis, Bangalore University, Bangalore, India